



HAL
open science

Dynamical correlations and screened exchange on the experimental bench: spectral properties of the cobalt pnictide BaCo_2As_2

Ambroise van Roekeghem, Thomas Ayrat, Jan Tomczak, Michele Casula, Nan Xu, Hong Ding, Michel Ferrero, Olivier Parcollet, Hong Jiang, Silke Biermann

► **To cite this version:**

Ambroise van Roekeghem, Thomas Ayrat, Jan Tomczak, Michele Casula, Nan Xu, et al.. Dynamical correlations and screened exchange on the experimental bench: spectral properties of the cobalt pnictide BaCo_2As_2 . *Physical Review Letters*, 2014, 113 (26), pp.266403. 10.1103/PhysRevLett.113.266403 . hal-02363989v2

HAL Id: hal-02363989

<https://hal.science/hal-02363989v2>

Submitted on 11 Nov 2024

HAL is a multi-disciplinary open access archive for the deposit and dissemination of scientific research documents, whether they are published or not. The documents may come from teaching and research institutions in France or abroad, or from public or private research centers.

L'archive ouverte pluridisciplinaire **HAL**, est destinée au dépôt et à la diffusion de documents scientifiques de niveau recherche, publiés ou non, émanant des établissements d'enseignement et de recherche français ou étrangers, des laboratoires publics ou privés.

Dynamical correlations and screened exchange on the experimental bench: spectral properties of the cobalt pnictide BaCo_2As_2

Ambroise van Roekeghem,^{1,2,*} Thomas Ayrat,^{2,3} Jan M. Tomczak,⁴ Michele Casula,⁵ Nan Xu,^{1,6} Hong Ding,^{1,7} Michel Ferrero,² Olivier Parcollet,³ Hong Jiang,⁸ and Silke Biermann^{2,9}

¹*Beijing National Laboratory for Condensed Matter Physics,*

and Institute of Physics, Chinese Academy of Sciences, Beijing 100190, China

²*Centre de Physique Théorique, Ecole Polytechnique, CNRS UMR 7644, 91128 Palaiseau, France*

³*Institut de Physique Théorique (IPhT), CEA, CNRS, URA 2306, 91191 Gif-sur-Yvette, France*

⁴*Institute of Solid State Physics, Vienna University of Technology, A-1040 Vienna, Austria*

⁵*CNRS and Institut de Minéralogie, de Physique des Matériaux et de Cosmochimie, Université Pierre et Marie Curie, case 115, 4 place Jussieu, FR-75252, Paris Cedex 05, France*

⁶*Swiss Light Source, Paul Scherrer Institut, CH-5232 Villigen, Switzerland*

⁷*Collaborative Innovation Center of Quantum Matter, Beijing, China*

⁸*College of Chemistry and Molecular Engineering, Peking University, 100871 Beijing, China*

⁹*Collège de France, 11 place Marcelin Berthelot, 75005 Paris, France*

(Dated: June 25, 2018)

Understanding the Fermi surface and low-energy excitations of iron or cobalt pnictides is crucial for assessing electronic instabilities such as magnetic or superconducting states. Here, we propose and implement a new approach to compute the low-energy properties of correlated electron materials, taking into account both screened exchange beyond the local density approximation and local dynamical correlations. The scheme allows us to resolve the puzzle of BaCo_2As_2 , for which standard electronic structure techniques predict a ferromagnetic instability not observed in nature.

PACS numbers: 71.27.+a, 71.45.Gm, 71.10.-w, 74.70.Xa, 79.60.-i

The discovery of unconventional superconductivity in iron pnictides and chalcogenides in 2008 has aroused strong interest into the Fermi surfaces and low-energy excitations of transition metal pnictides and related compounds. Angle-resolved photoemission spectroscopy (ARPES) has been used to systematically map out quasi-particle dispersions, and to identify electron and hole pockets potentially relevant for low-energy instabilities [1–7]. Density functional theory (DFT) calculations have complemented the picture, yielding information about orbital characters [8], or the dependence of the topology of the Fermi surface on structural parameters or element substitution [9, 10]. DFT within the local density approximation (LDA) or generalized gradient schemes has also served as a starting point for refined many-body calculations addressing band renormalizations and quasi-particle dispersions directly from a theoretical perspective (see e.g. Ref. [11–18]), and its combination with dynamical mean field theory (LDA+DMFT) [19–25] is nowadays the state-of-the-art *ab initio* many-body approach to low-energy properties of transition metal pnictides. Despite tremendous successes, however, limitations have also been pointed out e.g. in the description of the Fermi surfaces. Prominent examples include $\text{Ba}(\text{Fe},\text{Co})_2\text{As}_2$ [26, 27] or LiFeAs [14, 26]. Interestingly, many-body perturbation theory approximating the self-energy by its first order term in the screened Coulomb interaction W (so-called “ GW approximation”) results in a substantially improved description: calculations using the quasi-particle self-consistent (QS) GW method [28] have pinpointed non-local self-energy corrections to the

LDA Fermi surfaces not captured in LDA+DMFT as pivotal [26]. Yet, as a perturbative method, GW cannot be expected to describe materials away from the weak coupling limit [29], and the description of incoherent regimes [13, 17] including coherence-incoherence crossovers [30], local moment behavior [15] or the subtle effects of doping or temperature changes [17] are still reserved for DMFT.

In this Letter, we propose and implement a new approach to the spectral properties of correlated electron materials taking into account screened exchange beyond the local density approximation and correlations as described by dynamical mean field theory with frequency-dependent local Hubbard interactions. The approach can be understood as a simplified and extremely efficient version of the combined GW +DMFT method [31], as a non-perturbative dynamical generalization of the popular “Coulomb-Hole-Screened-EXchange” (COHSEX) scheme [32], or as a combination of generalized Kohn-Sham schemes [33, 34] with DMFT. We demonstrate the validity of our combined “Screened Exchange+dynamical DMFT” (“SEx+DDMFT”) scheme by calculating the spectral function of BaCo_2As_2 for which detailed ARPES results are available [35, 36]. Finally, our work sheds new light on the physical justifications of electronic structure techniques that combine density functional with dynamical mean field theory, by revealing a subtle error cancellation between non-local exchange interactions and dynamical screening effects, both neglected in standard methods.

Our target compound, BaCo_2As_2 , is isostructural to the prototypical parent compound of the so-called 122

iron-based superconductors, BaFe_2As_2 . Replacing Fe by Co, however, increases the filling to a nominal d^7 configuration of the 3d states, with drastic consequences: whereas compounds with filling around the d^6 configuration exhibit characteristic power law deviations from Fermi liquid behavior above often extremely low coherence temperatures [17], in the d^7 compound BaCo_2As_2 ARPES identifies clearly defined long-lived quasi-particle bands with relatively weak mass renormalizations [35]. Nevertheless, the electronic structure of this compound raises puzzling questions concerning its paramagnetic behavior. Indeed, standard electronic structure calculations predict a huge density of states at the Fermi level, which, given the large Stoner parameter of Co, would be expected to trigger an instability towards a ferromagnetic state [37]. The density of states of the iso-electronic compound SrCo_2As_2 presents the same features, but the maximum appears to be just below the Fermi level [38]. Still, in SrCo_2As_2 – also a paramagnet – important antiferromagnetic fluctuations have been measured, possibly competing with ferromagnetic order [38, 39]. CaCo_2As_2 , $\text{Ca}_{0.9}\text{Sr}_{0.1}\text{Co}_2\text{As}_2$ and $\text{CaCo}_{1.86}\text{As}_2$ exhibit magnetic phases with in-plane ferromagnetism at low temperatures [40–42]. ARPES data of BaCo_2As_2 show that there is indeed a flat band (dominantly of $d_{x^2-y^2}$ character) very close to the Fermi surface, albeit less filled than predicted by LDA calculations [35, 36], suggesting BaCo_2As_2 to be on the verge of a transition [53]. These properties make the compound an ideal benchmark system, on which to test new theoretical approaches.

We start our analysis by comparing results for the spectral function calculated within different state-of-the-art electronic structure techniques to the ARPES spectral function of Ref. [35] (Fig. 1). Specifically, we analyze the Kohn-Sham band structure of DFT-LDA and the spectral functions of standard LDA+DMFT and LDA+DMFT with frequency-dependent local Hubbard interactions $\mathcal{U}(\omega)$. The latter scheme will be abbreviated in the following as “LDA+DDMFT” to stress the doubly dynamical nature of the theory, which determines a frequency-dependent self-energy in the DMFT spirit but does so extending DMFT to frequency-dependent interactions. Details of the scheme can be found in Refs. [17, 43] and the supplementary material. The effective local interactions used in the DMFT calculations were obtained within the constrained random phase approximation in the implementation of [44]. For LDA+DDMFT, the full frequency-dependence of the monopole term, $F_0(\omega)$ (see supplementary) is retained in the calculation. The effective local problem with dynamical \mathcal{U} is solved self-consistently by means of a continuous-time Monte Carlo algorithm [45, 46] that we have implemented within the TRIQS toolbox [47].

Electronic bands in the energy window between the Fermi level and -2 eV binding energy are states of pre-

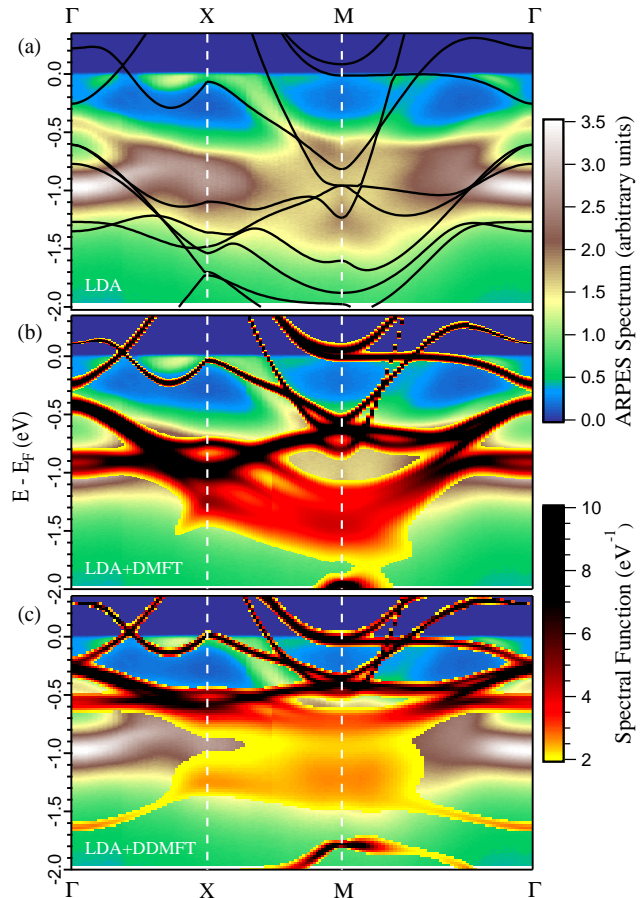


Figure 1: BaCo_2As_2 photoemission spectra, replotted from Ref. [35]. Superimposed are (a) the Kohn-Sham band structure of DFT-LDA (b) spectral function of standard LDA+DMFT [only those parts that exceed 2 states/eV are shown] (c) spectral function within LDA+DDMFT [same representation as in (b)].

dominant Co-3d character, and undergo – even in this quite moderately correlated compound – a non-negligible band renormalization, as compared to the LDA band structure (Fig. 1 (a)). Standard LDA+DMFT (Fig. 1 (b)) captures this effect, leading to a reduced bandwidth in good agreement with the ARPES results. When dynamical screening effects are taken into account (Fig. 1 (c)), additional renormalizations occur, corresponding to the electronic polaron effect discussed in Ref. [48], and the overall bandwidth reduction appears to be overestimated. We will, however, argue below that one should not conclude from this analysis that dynamical screening effects are absent. Rather, non-local exchange – routinely neglected in DFT-based techniques – reshapes and widens the quasi-particle band structure, and the apparent success of LDA+DMFT in obtaining the correct quasi-particle bandwidth relies on an error cancellation when both dynamical screening and non-local exchange are neglected in the calculation of the spectral

function. We will now substantiate this claim by explicitly including screened exchange, and performing a DMFT calculation with fully dynamical Hubbard interactions based on the following one-particle Hamiltonian: $H_0 = H_{Hartree} + H_{SEx}$ where the first term denotes the Hamiltonian of the system at the Hartree mean-field level, evaluated at the self-consistent DFT-LDA density. H_{SEx} is a screened Fock exchange term, calculated from the Yukawa potential $\frac{e^2 \exp(-k_{TF}|r-r'|)}{|r-r'|}$ with screening wavevector k_{TF} (see supplementary). This scheme can be understood as the next generation after the recent LDA+DDMFT scheme, by replacing the local Kohn-Sham exchange-correlation potential of DFT by a non-local screened Fock exchange correction [54].

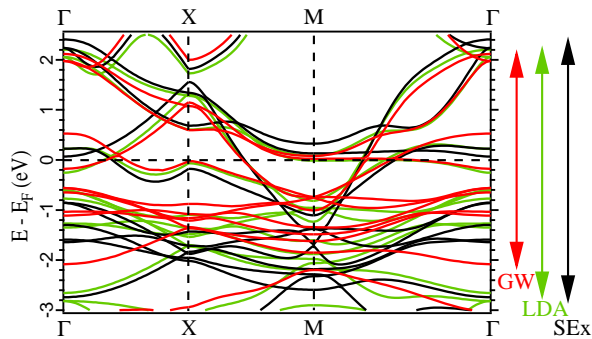


Figure 2: Comparison of bandstructures of BaCo_2As_2 in the $k_z = 0$ plane calculated within QSGW (red), LDA (green) and Screened-Exchange (black).

We first analyze the band structure corresponding to H_0 alone, in comparison to the LDA band structure and the one obtained from QSGW (in the implementation of [49]), see Fig. 2. As expected, the inclusion of non-local exchange in H_0 increases the delocalization of electrons, particularly for the bands crossing the Fermi level, and thus widens them as compared to the LDA electronic structure. In QSGW, this effect is overcompensated by correlation-induced band-narrowing, and the bandwidth of Cobalt d -like bands is about 15 % smaller than in LDA. These comparisons highlight the fact that – taking the screened exchange band structure as a reference – the effective exchange-correlation potential of DFT not only incorporates exchange (in a local fashion), but also mimics band renormalizations due to correlations (yet without keeping track of the corresponding spectral weight transfers). In addition, the SEx correction induces interesting modifications of the low-energy band structure as compared to the LDA; we will come back to this point below.

We finally turn to the results of our new scheme: Fig. 3 displays the spectral function within “SEx+DDMFT”. Panel (b) displays again the ARPES data, but this time the maxima of the SEx+DDMFT spectral function are superimposed to the color spectrum. The overall spec-

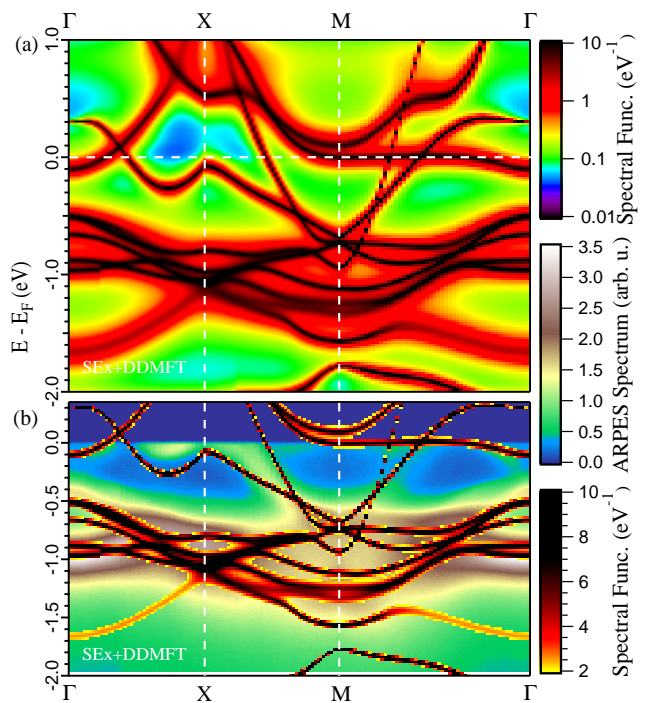


Figure 3: BaCo_2As_2 within Screened Exchange+DDMFT: (a) spectral function (b) bands extracted from the maxima of panel (a) and superimposed on ARPES data as in Fig. 1.

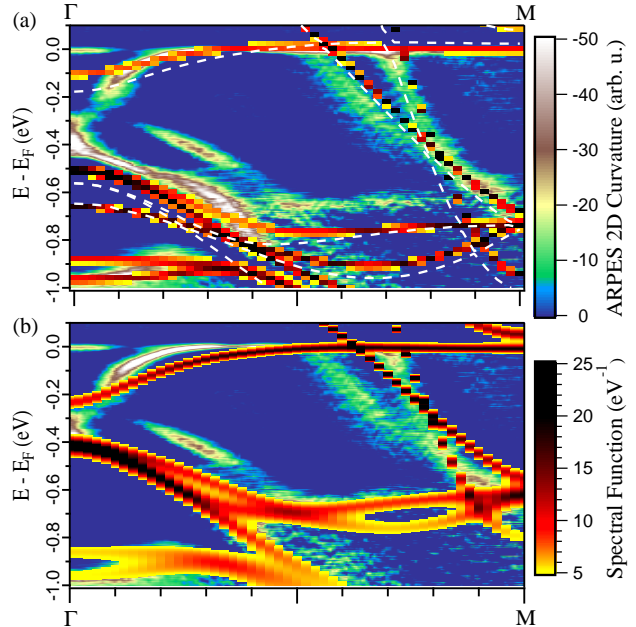


Figure 4: Bands along the ΓM direction, extracted from the spectral function calculated by (a) SEx+DDMFT and (b) LDA+DMFT, superimposed on ARPES data from Ref. [35] (represented as a second derivative of the photoemission intensity). The QSGW band structure is also given (white dashed lines).

trum from SE_x+DDMFT is very close to the experiment: bandwidth, Fermi surface and band renormalizations close to the Fermi level are correctly predicted.

Table I: Number of electrons in Cobalt-*d* Wannier functions within the LDA, SE_x, SE_x+DDMFT, LDA+DMFT and LDA+DDMFT.

	n_{LDA}^{e-}	$n_{\text{SE}_x}^{e-}$	$n_{\text{SE}_x+\text{DDMFT}}^{e-}$	$n_{\text{LDA}+\text{DMFT}}^{e-}$	$n_{\text{LDA}+\text{DDMFT}}^{e-}$
d_{z^2}	1.64	1.66	1.63	1.61	1.62
$d_{x^2-y^2}$	1.49	1.27	1.37	1.53	1.59
d_{xy}	1.74	1.78	1.72	1.67	1.63
d_{xz+yz}	1.69	1.73	1.68	1.64	1.62
total	8.24	8.16	8.08	8.09	8.09

The orbital-resolved electron count obtained with SE_x+DDMFT is displayed in Tab. I and compared to the LDA, SE_x, LDA+DMFT and LDA+DDMFT electron count. The orbital polarization from LDA is reduced by correlations, and nearly suppressed within LDA+DDMFT. Conversely, screened exchange increases the orbital polarization, and the final SE_x+DDMFT result still displays stronger orbital polarization than LDA. This trend can be directly related to the weakly dispersive $d_{x^2-y^2}$ states discussed above: as in the SE_x band dispersion of Fig. 2, the effect of screened exchange is to push the flat $d_{x^2-y^2}$ -like band away from the Fermi level, to the point of suppressing the electron pocket at the Γ point. This does not correspond to the experimental spectrum, and indeed it is corrected by including correlations. Fig. 4 displays the low-energy spectra along the ΓM direction comparing SE_x+DDMFT and LDA+DMFT overlaid onto the second derivative of the ARPES data [50], together with the QSGW band dispersion. The electron pocket at Γ is recovered in SE_x+DDMFT, and the fraction of $d_{x^2-y^2}$ electrons increases. Within LDA, the flat band is nearly filled along the ΓM direction, and even more so when we take into account correlations. According to ARPES, this flat band should be occupied only in a small electron pocket at Γ , containing about 0.18 e^- . This result is consistent with the absence of ferromagnetism. Indeed, this flat band lying on the Fermi surface would imply a high density of states at the Fermi level that could trigger a Stoner instability. We extract from the SE_x+DDMFT calculations a DOS at the Fermi energy of 0.97 states/eV/Co/spin. Assuming a Stoner parameter of ~ 0.9 eV this leaves us slightly below the onset of Stoner ferromagnetism [55]. The QSGW scheme also provides an overall good description, including the position of the $d_{x^2-y^2}$ band, its filling and its related Fermi wavevector. Taking non-local exchange into account is thus necessary to capture the physics of BaCo₂As₂, and our SE_x+DDMFT scheme performs well for these subtle effects.

Finally, a few comments are in order to put our new computational scheme into perspective. As far as coarse

features such as the bandwidth are concerned, standard LDA+DMFT and the new SE_x+DDMFT give comparable results, giving an *a posteriori* explanation for the success of LDA+DMFT calculations with static interactions. For total energy calculations within DFT, it is well-known that there are subtle error cancellations between the exchange and correlation contributions in approximate density functionals. Here, we evidence a similar behavior for spectral properties. The effect of dynamical screening as incorporated in the high-energy tail of the dynamical Hubbard interaction $\mathcal{U}(\omega)$ can roughly be understood by a band narrowing by a factor $Z_B = \exp(-\int_0^\infty d\omega \Im \mathcal{U}(\omega)/(\pi\omega^2))$ [56]. For BaCo₂As₂, we find dynamical screening to be non-negligible, with $Z_B \sim 0.6$. LDA+DDMFT doublecounts this narrowing effect, as the bandwidth has already been decreased by correlations hidden in the effective exchange-correlation potential of DFT, with respect to the Hartree-Fock or SE_x bandstructure (see Fig. 2). Thus, starting a many-body calculation from LDA raises not only the usual well-known double counting questions related to the energetic position of correlated versus itinerant states, but even more serious ones related to the double counting of screening processes. Our SE_x+DDMFT scheme avoids these issues, providing a more solid foundation for the investigation of dynamical screening effects. On a more pragmatic level, the similarity of the LDA+DMFT and SE_x+DDMFT spectral functions also suggests that error cancellations between dynamical screening and non-local exchange, both absent in LDA+DMFT, make this scheme suitable at least for questions concerning the overall bandwidth reduction of correlated electron systems. Finer details related to the very low energy behavior or Fermi surface topologies, on the other hand, might require explicit exchange corrections as introduced in the present work.

In summary, we have shown that screened exchange combined with dynamical correlations provides an excellent description of the low-energy physics in BaCo₂As₂. In contrast to perturbative schemes, it can be expected that our non-perturbative method can be extended to regimes with arbitrarily strong correlations, making it a promising tool for probing the finite temperature normal state of iron pnictide and chalcogenide superconductors. For BaCo₂As₂, we show that the flat $d_{x^2-y^2}$ -band in the immediate vicinity of the Fermi level is extremely sensitive to an accurate treatment of screened exchange, and that this effect is key to the paramagnetic nature of the compound. Pump-probe photoemission would be useful to experimentally locate the flat band and guide the search for new ways to tune its exact energetic position, thus directly playing on possible Fermi surface instabilities.

We acknowledge useful discussions with V. Brouet, T. Miyake and the authors of Ref. [35]. This work was supported by the French ANR under project PNICTIDES,

IDRIS/GENCI under projects 91393 and 96493, the Cai Yuanpei program, and the European Research Council (projects number 617196 and 278472). JMT acknowledges hospitality of CPHT within a CNRS visiting position. HJ acknowledges the support by the National Natural Science Foundation of China (Projects Nos. 20973009 and 21173005).

* Electronic address: vanroeke@cpht.polytechnique.fr

- [1] H. Ding, P. Richard, K. Nakayama, K. Sugawara, T. Arakane, Y. Sekiba, A. Takayama, S. Souma, T. Sato, T. Takahashi, et al., *EPL* **83**, 47001 (2008).
- [2] C. Liu, G. D. Samolyuk, Y. Lee, N. Ni, T. Kondo, A. F. Santander-Syro, S. L. Bud'ko, J. L. McClesney, E. Rotenberg, T. Valla, et al., *Phys. Rev. Lett.* **101**, 177005 (2008).
- [3] V. Brouet, M. Marsi, B. Mansart, A. Nicolaou, A. Taleb-Ibrahimi, P. Le Fèvre, F. Bertran, F. Rullier-Albenque, A. Forget, and D. Colson, *Phys. Rev. B* **80**, 165115 (2009).
- [4] T. Shimojima, K. Ishizaka, Y. Ishida, N. Katayama, K. Ohgushi, T. Kiss, M. Okawa, T. Togashi, X.-Y. Wang, C.-T. Chen, et al., *Phys. Rev. Lett.* **104**, 057002 (2010).
- [5] S. de Jong, Y. Huang, R. Huisman, F. Masseur, S. Thirupathaiiah, M. Gorgoi, F. Schaefer, R. Follath, J. B. Goedkoop, and M. S. Golden, *Phys. Rev. B* **79**, 115125 (2009).
- [6] J. Fink, S. Thirupathaiiah, R. Ovsyannikov, H. A. Dürr, R. Follath, Y. Huang, S. de Jong, M. S. Golden, Y.-Z. Zhang, H. O. Jeschke, et al., *Phys. Rev. B* **79**, 155118 (2009).
- [7] W. Malaeb, T. Yoshida, A. Fujimori, M. Kubota, K. Ono, K. Kihou, P. M. Shirage, H. Kito, A. Iyo, H. Eisaki, et al., *J. Phys. Soc. Jpn.* **78**, 123706 (2009).
- [8] D. J. Singh, *Physica C: Superconductivity* **469**, 418 (2009).
- [9] V. Vildosola, L. Pourovskii, R. Arita, S. Biermann, and A. Georges, *Phys. Rev. B* **78**, 064518 (2008).
- [10] I. I. Mazin, D. J. Singh, M. D. Johannes, and M. H. Du, *Phys. Rev. Lett.* **101**, 057003 (2008).
- [11] K. Haule, J. H. Shim, and G. Kotliar, *Phys. Rev. Lett.* **100**, 226402 (2008).
- [12] M. Aichhorn, L. Pourovskii, V. Vildosola, M. Ferrero, O. Parcollet, T. Miyake, A. Georges, and S. Biermann, *Phys. Rev. B* **80**, 085101 (2009).
- [13] M. Aichhorn, S. Biermann, T. Miyake, A. Georges, and M. Imada, *Phys. Rev. B* **82**, 064504 (2010).
- [14] J. Ferber, K. Foyevtsova, R. Valentí, and H. O. Jeschke, *Phys. Rev. B* **85**, 094505 (2012).
- [15] P. Hansmann, R. Arita, A. Toschi, S. Sakai, G. Sangiovanni, and K. Held, *Phys. Rev. Lett.* **104**, 197002 (2010).
- [16] V. I. Anisimov, D. Korotin, M. Korotin, A. V. Kozhevnikov, J. Kunes, A. O. Shorikov, S. L. Skornyakov, and S. V. Streltsov, *J. Phys. Condens. Matter* **21**, 075602 (2009).
- [17] P. Werner, M. Casula, T. Miyake, F. Aryasetiawan, A. J. Millis, and S. Biermann, *Nature Physics* **8**, 331 (2012).
- [18] G. Wang, Y. Qian, G. Xu, X. Dai, and Z. Fang, *Phys. Rev. Lett.* **104**, 047002 (2010).
- [19] V. I. Anisimov, A. Poteryaev, M. Korotin, A. Anokhin, and G. Kotliar, *J. Phys. Condens. Matter* **9**, 7359 (1997).
- [20] A. I. Lichtenstein and M. I. Katsnelson, *Phys. Rev. B* **57**, 6884 (1998).
- [21] G. Kotliar and D. Vollhardt, *Physics Today* **57**, 53 (2004).
- [22] S. Biermann, in *Encyclopedia of Materials: Science and Technology*, edited by K. H. J. Buschow, R. W. Cahn, M. C. Flemings, B. Ilschner (print), E. J. Kramer, S. Mahajan, and P. Veyssi ere (updates) (Elsevier, Oxford, 2006), pp. 1 – 9.
- [23] K. Held, I. A. Nekrasov, G. Keller, V. Eyert, N. Bl umer, A. K. McMahan, R. T. Scalettar, T. Pruschke, V. I. Anisimov, and D. Vollhardt, *physica status solidi (b)* **243** (2006), *psi-k Newsletter*, 56 (65) 2003.
- [24] G. Kotliar, S. Y. Savrasov, K. Haule, V. S. Oudovenko, O. Parcollet, and C. A. Marianetti, *Rev. Mod. Phys.* **78**, 865 (2006).
- [25] J. Min ar, L. Chioncel, A. Perlov, H. Ebert, M. I. Katsnelson, and A. I. Lichtenstein, *Phys. Rev. B* **72**, 045125 (2005).
- [26] J. M. Tomczak, M. van Schilfgaarde, and G. Kotliar, *Phys. Rev. Lett.* **109**, 237010 (2012).
- [27] V. Brouet, P.-H. Lin, Y. Texier, J. Bobroff, A. Taleb-Ibrahimi, P. Le F evre, F. Bertran, M. Casula, P. Werner, S. Biermann, et al., *Phys. Rev. Lett.* **110**, 167002 (2013).
- [28] M. van Schilfgaarde, T. Kotani, and S. Faleev, *Phys. Rev. Lett.* **96**, 226402 (2006).
- [29] T. Ayr al, P. Werner, and S. Biermann, *Phys. Rev. Lett.* **109**, 226401 (2012).
- [30] K. Haule and G. Kotliar, *New J. Phys.* **11**, 025021 (2009).
- [31] S. Biermann, F. Aryasetiawan, and A. Georges, *Phys. Rev. Lett.* **90**, 086402 (2003).
- [32] L. Hedin, *Phys. Rev.* **139**, A796 (1965).
- [33] D. M. Bylander and L. Kleinman, *Phys. Rev. B* **41**, 7868 (1990).
- [34] A. Seidl, A. G orling, P. Vogl, J. A. Majewski, and M. Levy, *Phys. Rev. B* **53**, 3764 (1996).
- [35] N. Xu, P. Richard, A. van Roekeghem, P. Zhang, H. Miao, W.-L. Zhang, T. Qian, M. Ferrero, A. S. Sefat, S. Biermann, et al., *Phys. Rev. X* **3**, 011006 (2013).
- [36] R. S. Dhaka, Y. Lee, V. K. Anand, D. C. Johnston, B. N. Harmon, and A. Kaminski, *Phys. Rev. B* **87**, 214516 (2013).
- [37] A. S. Sefat, D. J. Singh, R. Jin, M. A. McGuire, B. C. Sales, and D. Mandrus, *Phys. Rev. B* **79**, 024512 (2009).
- [38] A. Pandey, D. G. Quirinale, W. Jayasekara, A. Sapkota, M. G. Kim, R. S. Dhaka, Y. Lee, T. W. Heitmann, P. W. Stephens, V. Ogloblich, et al., *Phys. Rev. B* **88**, 014526 (2013).
- [39] W. Jayasekara, Y. Lee, A. Pandey, G. S. Tucker, A. Sapkota, J. Lamsal, S. Calder, D. L. Abernathy, J. L. Niedziela, B. N. Harmon, et al., *Phys. Rev. Lett.* **111**, 157001 (2013).
- [40] B. Cheng, B. F. Hu, R. H. Yuan, T. Dong, A. F. Fang, Z. G. Chen, G. Xu, Y. G. Shi, P. Zheng, J. L. Luo, et al., *Phys. Rev. B* **85**, 144426 (2012).
- [41] J. J. Ying, Y. J. Yan, A. F. Wang, Z. J. Xiang, P. Cheng, G. J. Ye, and X. H. Chen, *Phys. Rev. B* **85**, 214414 (2012).
- [42] V. K. Anand, R. S. Dhaka, Y. Lee, B. N. Harmon, A. Kaminski, and D. C. Johnston, *Phys. Rev. B* **89**, 214409 (2014).
- [43] M. Casula, A. Rubtsov, and S. Biermann, *Phys. Rev. B*

- 85**, 035115 (2012).
- [44] L. Vaugier, H. Jiang, and S. Biermann, Phys. Rev. B **86**, 165105 (2012).
- [45] P. Werner, A. Comanac, L. de' Medici, M. Troyer, and A. J. Millis, Phys. Rev. Lett. **97**, 076405 (2006).
- [46] P. Werner and A. J. Millis, Phys. Rev. Lett. **104**, 146401 (2010).
- [47] M. Ferrero and O. Parcollet, *TRIQS: A toolbox for research on interacting quantum systems* (2011), <http://ipht.cea.fr/triqs>.
- [48] M. Casula, P. Werner, L. Vaugier, F. Aryasetiawan, T. Miyake, A. J. Millis, and S. Biermann, Phys. Rev. Lett. **109**, 126408 (2012).
- [49] T. Kotani, M. van Schilfgaarde, and S. V. Faleev, Phys. Rev. B **76**, 165106 (2007).
- [50] P. Zhang, P. Richard, T. Qian, Y.-M. Xu, X. Dai, and H. Ding, Rev. Sci. Instrum. **82**, 043712 (2011).
- [51] J. M. Tomczak, M. Casula, T. Miyake, and S. Biermann, Phys. Rev. B **90**, 165138 (2014).
- [52] J. M. Tomczak, M. Casula, T. Miyake, F. Aryasetiawan, and S. Biermann, EPL **100**, 67001 (2012).
- [53] Indeed, a presentation of the ARPES spectra in a second derivative plot of the intensities reveals the presence of a flat band just above the Fermi level [35], as pointed out in Ref. [36].
- [54] We note that in SEx+DMFT non-local and dynamical renormalizations are by construction separated on the self-energy/Hamiltonian level. This separability was recently justified for iron pnictides [26] and found to hold also for metallic transition metal oxides [51, 52].
- [55] However, slight electron doping would bring us close to the maximum value of 1.04 states/eV/Co/spin that we find at $\omega = 44\text{meV}$, at the peak of the Co $d_{x^2-y^2}$ DOS, possibly triggering a ferromagnetic instability.
- [56] In the anti-adiabatic limit, where the characteristic frequency of variations in $\mathcal{U}(\omega)$ is larger than the other energy scales of the system, this statement can be made rigorous by means of a Lang-Firsov transformation, as demonstrated in Ref. [48].
-

Dynamical correlations and screened exchange on the experimental bench: spectral properties of the cobalt pnictide BaCo₂As₂ - Supplementary material

In this supplementary material, we give further details explaining the motivation, implementation and technical aspects of the proposed combined Screened Exchange Dynamical Mean Field scheme with Dynamical interactions “SEx+DDMFT”.

I. THE COMBINED SCREENED EXCHANGE DYNAMICAL MEAN FIELD (SEX+DMFT) SCHEME

A. Motivation and general idea

The screened exchange dynamical mean field technique “SEx+DDMFT” is motivated by the observation that the first non-local corrections to standard LDA+DMFT can be understood as screened exchange terms. Indeed, within the *GW* approximation (GWA) it has been shown recently [S1, S2] that for whole classes of materials (the focus was in particular on iron pnictides), the *GW* correction to LDA can be split into two contributions: a dynamical but local self-energy $\Sigma_{loc}(\omega)$ and a k-dependent but static self-energy $\Sigma_{nloc}(k)$. Obviously, if such a separation were strictly valid over all energies, the static contribution would be given by the Hartree-Fock self-energy, since the dynamical part of the self-energy vanishes at high frequency. However, in reality, such a decomposition holds to a good approximation in the low-energy regime that we are interested in, with a static offset $\Sigma_{nloc}(k)$ which is quite different from the Fock exchange term. Here, we identify this contribution as a screened exchange self-energy, leading to a decomposition of the *GW* self-energy $\Sigma_{GW}(k, \omega) = i \sum_{\nu, q} G(k+q, \omega+\nu)W(q, \nu)$ into $\Sigma_{GW}(k, \omega) = GW(\nu=0) + [GW]_{local}$ where the first term is a screened exchange contribution arising from the screened interaction *W* evaluated at zero frequency. In the practical implementation we replace it by its long-wavelength limit: in this $q \rightarrow 0$ limit, the RPA-screened Coulomb potential *W* reduces to a simple Yukawa-form, which we discuss below. Within the GWA, the dynamical local term is simply given by a *GW* self-energy evaluated using a local propagator G_{local} and the local screened Coulomb interaction W_{local} . In the SEx+DDMFT scheme, however, we go a decisive step further and evaluate this term from a dynamical impurity problem as in DDMFT. In contrast to the GWA, it is therefore determined non-perturbatively. For weakly correlated materials such as BaCo₂As₂ we expect the GWA to be quite accurate, and the non-perturbative and the perturbative evaluation should qualitatively coincide. This corresponds indeed to our finding of SEx+DDMFT results being close to the *GW* ones (see main text). The SEx+DDMFT is however not limited to this case, mak-

ing it a promising perspective for investigations in the strongly correlated metal regime.

B. Formulation

Thanks to its static nature, the screened exchange self-energy correction to the LDA Hamiltonian can be directly incorporated into a revised one-particle Hamiltonian $H_0 = H_{LDA} - V_{xc}^{LDA} + V_{SEx}$. The SEx+DDMFT scheme then consists in performing DDMFT starting from the general multi-orbital Hamiltonian $H = H_0 + H_{int} - H_{dc}$ where H_{int} is the dynamical generalization of the usual Hubbard and Hund interaction terms. To indeed be able to write it in a Hamiltonian fashion, we decompose it into a static part which we restrict to density-density-interactions $H_{intstat} = \frac{1}{2} \sum_i \sum_{m\sigma \neq m'\sigma'} U_{m\sigma m'\sigma'} (\nu = \infty) n_{im\sigma} n_{im'\sigma'}$ (where the sums i, j run over the Co-3*d* orbitals) and an additional part introducing screening bosons and their coupling to the physical electrons: $H_{screening} = \sum_i \int_{\omega} d\omega \left[\lambda_{\omega} \sum_{m\sigma} n_{im\sigma} (b_{i,\omega}^{\dagger} + b_{i,\omega}) + \omega (b_{i,\omega}^{\dagger} b_{i,\omega} + \frac{1}{2}) \right]$. Such a formulation has been discussed in the recent generalization of LDA+DMFT to dynamical Hubbard interactions in Refs.[S3, S4]. Alternatively, if an action formulation is chosen, H_{int} corresponds to the Hubbard interactions where the monopole term (the Slater integral F_0) is frequency-dependent. H_{dc} is the double-counting correction introduced in order to remove from the screened exchange Hamiltonian those contributions of the interaction that are explicitly treated in a many-body fashion in the form of H_{int} . For details, see Section IE.

C. Screened exchange term and screening length

The screened exchange contribution H_{SEx} is calculated as Fock exchange with the screened potential $W^{RPA}(q \rightarrow 0, \nu=0) \rightarrow \frac{e^2}{4\pi\epsilon_0} \frac{4\pi}{q^2 + k_{TF}^2}$. Here, k_{TF} is the Thomas-Fermi wavevector or inverse screening length. It can be expressed as $k_{TF}^2 \equiv -e^2 \epsilon_0^{-1} P^0(q=0, \nu=0)$ where – in a metallic system such as BaCo₂As₂ – the static polarization $P^0(0,0)$ is well approximated by the one of the homogeneous electron gas at low temperature $k_B T \ll \epsilon_F$: $P^0(0,0) \rightarrow -\rho(\epsilon_F)$. The problem of calculating the screened exchange term therefore boils down to determining the effective screening length. Starting from the LDA DOS (6.94 states/eV/unit cell), we obtain a screening wavevector of 1.88 a_0^{-1} , with a_0 the Bohr radius. However, as argued above, one of the main consequences of the electronic exchange and correlation effects is precisely

the rearrangement of the electronic states in the immediate proximity of the Fermi level, and a concomitant reduction of the density of states. Indeed, a SEx+DDMFT calculation with the LDA screening length results in a reduction of states at the Fermi level, given by a zero-frequency spectral function of 4.66 states/eV/unit cell, corresponding to a screening wavevector of $1.54 a_0^{-1}$. It thus becomes clear that the true challenge consists in a *self-consistent* determination of the effective screening length. For computational reasons, however, and since the precise value of the DOS at the Fermi level is – for the same reasons as the subtle Fermi surface modifications discussed above – a quantity very hard to converge, we mimic convergence by choosing an ad hoc screening wavevector of $1.33 a_0^{-1}$, corresponding to half the LDA-DOS. Since this is approximately the value we eventually find for the value of the spectral function on the Fermi level (4.26 states/eV/cell – which corresponds to about $1.47 a_0^{-1}$), this choice can be considered as a poor man’s self-consistency.

For the screened Hartree-Fock calculation performed within Wien2k [S5, S6], we calculate the matrix-elements for a second variational procedure on 150 bands, on a grid of $7 \times 7 \times 7$ k-points.

D. Interactions

1. Static Hubbard and Hund Interactions

The interactions are determined from the constrained random phase approximation (cRPA) in the implementation of [S7]. In the zero-frequency limit, we obtain the Slater integrals $F^0(0) = 2.9$, $F^2(0) = 6.9$ and $F^4(0) = 5.1$ calculated on a grid of $4 \times 4 \times 4$ k-points, which we use to determine the orbital-dependent coefficients $U_{mm'}$ of density-density interactions, including Hund’s exchange $J_{mm'}$, in a standard Slater parametrisation [S8]. We find $J = 0.86$ and the interaction matrices in the cubic basis d_{z^2} , $d_{x^2-y^2}$, d_{xy} , d_{xz} , d_{yz} at $\omega = 0$:

$$\bar{U}_{mm'}^{\sigma\sigma'}|_{\text{Slater}} = \begin{pmatrix} 0 & 1.66 & 1.66 & 2.41 & 2.41 \\ 1.66 & 0 & 2.66 & 1.91 & 1.91 \\ 1.66 & 2.66 & 0 & 1.91 & 1.91 \\ 2.41 & 1.91 & 1.91 & 0 & 1.91 \\ 2.41 & 1.91 & 1.91 & 1.91 & 0 \end{pmatrix}$$

$$\bar{U}_{mm'}^{\sigma\bar{\sigma}}|_{\text{Slater}} = \begin{pmatrix} 3.87 & 2.40 & 2.40 & 2.90 & 2.90 \\ 2.40 & 3.87 & 3.06 & 2.56 & 2.56 \\ 2.40 & 3.06 & 3.87 & 2.73 & 2.56 \\ 2.90 & 2.56 & 2.56 & 3.87 & 2.56 \\ 2.90 & 2.56 & 2.56 & 2.56 & 3.87 \end{pmatrix}.$$

2. Dynamical interactions

The cRPA method also gives us access to the frequency-dependence of the interactions.

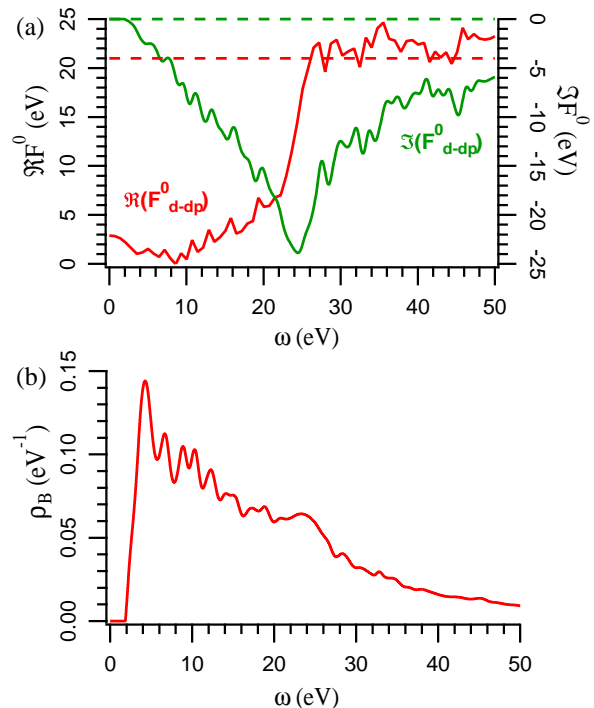


Figure S1: (a) Frequency-dependent real and imaginary parts of the monopole screened Coulomb interaction $F_{d-dp}^0(\omega)$; (b) Corresponding bosonic spectral function $\rho_B(\omega)$.

The full frequency-dependent monopole integral $F^0(\omega)$ is displayed in Figure S1, along with the corresponding bosonic spectral function $\rho_B(\omega)$ with the notations of Ref. [S9]. The imaginary part of F^0 has a minimum around 22 eV, which corresponds to the main plasmon. At this frequency the real part of F^0 is multiplied by 4, going from a low-frequency regime to a high-frequency regime. Still, a non-trivial frequency dependence persists at lower frequencies, and that is why the spectrum of ρ_B shows many features and a broad repartition of the spectral weight. Formally, the bosonic renormalization factor (within the notations of Ref. [S4]) would be $Z_B=0.59$.

E. Double-counting

The Hubbard Hamiltonian used in DMFT contains a Hartree term. However, the Hartree energy from the input (whether it is LDA or calculated from a Yukawa potential) is already taken into account in the DFT part. For this reason, one needs to introduce a correction term introduced to avoid double-counting part of the Coulomb interactions. Here, we use an orbital-

dependent double counting term derived as a mean field approximation of the Hubbard terms: $V_{DC}(m, \sigma) = \sum_{m', \sigma' \neq m, \sigma} U(m\sigma, m'\sigma') \langle n_{m'\sigma'} \rangle_{DFT}$. We note that in the absence of orbital polarization one would recover the usual “around mean field” (AMF) formula [S10]. The values of $\langle n_{m'\sigma'} \rangle_{DFT}$ are taken from the DFT starting point – the LDA or SE x calculation.

Table I: Orbital-resolved value of double-counting for LDA and SE x , and effective mass of Cobalt- d Wannier functions in SE x +DDMFT, LDA+DMFT and LDA+DDMFT.

	DC_{LDA}	DC_{SEx}	$m_{SEx+U(\omega)}^*$	$m_{LDA+U(0)}^*$	$m_{LDA+U(\omega)}^*$
d_{z^2}	18.665	18.552	1.74	1.26	1.95
$d_{x^2-y^2}$	18.493	18.159	1.86	1.27	1.90
d_{xy}	18.719	18.628	1.68	1.25	1.94
d_{xz}/d_{yz}	18.599	18.415	1.68	1.24	1.90

The values of the double counting term are displayed in Table I.

F. Screened EXchange+Dynamical Mean Field Theory: Link to GW +DMFT and COHSEX

The above decomposition of the self-energy, which essentially consists in singling out the local term, is reminiscent of the combined GW +DMFT scheme [S11], in which local and non-local parts of the self-energy are treated within DMFT and GW respectively. Indeed, the SE x +DMFT scheme can be understood as a simplified version of GW +DMFT, where the non-local self-energy is approximated by the screened exchange term.

Alternatively, the SE x +DDMFT scheme can also be understood as a dynamical generalization of Hedin’s Coulomb-hole-screened-exchange (COHSEX) approximation [S12]. In that scheme, a static approximation to the self-energy is constructed from two terms: first, a screened exchange term analogous to the one we treat here, and second the Coulomb-hole, a local correction expressing the suppression of the charge-charge correlator in the vicinity of an electron. In SE x +DDMFT, the latter term is determined in a dynamical and non-perturbative manner from a local impurity model (that is, by DMFT with dynamical interactions).

II. ADDITIONAL RESULTS ON $BaCo_2As_2$

In this section, we give additional information on our SE x +DDMFT results, concerning the momentum-integrated spectral function as well as the very low-energy behavior related to the flat band at the Fermi surface.

A. Momentum-integrated cobalt-3d spectral function

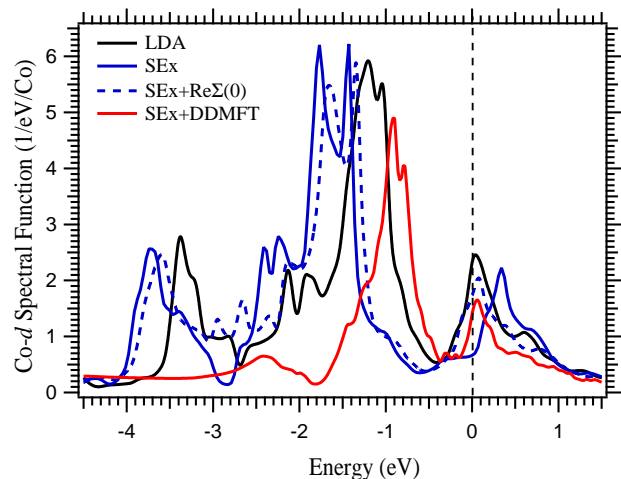


Figure S2: Cobalt- d spectral function from SE x +DDMFT (red) compared to the Co- d density of states within LDA (black), SE x (solid blue lines), and SE x shifted by the real part of the self-energy at zero frequency (dashed blue lines).

Figure S2 displays the momentum-integrated Co-3 d spectral function within the different schemes: LDA, SE x , and SE x +DDMFT. Also shown is the density of states corresponding to an intermediate level of sophistication, namely resulting from SE x shifted by the orbital-dependent self-energy matrix at zero frequency. Although a purely auxiliary quantity, this density of states is interesting, since the full SE x +DDMFT spectral function differs from it only through a self-energy correction that vanishes on the Fermi level. For this reason, the value on the Fermi level of the two quantities coincide, up to finite temperature effects encoded in the imaginary part of the self-energy (and, of course, numerical limitations). However, this value is strongly reduced compared to the initial LDA DOS, as a consequence of the exchange-enlarged bandwidth. The new value is consistent with the absence of ferromagnetism, as discussed in the main text.

B. Low-energy behavior along the ΓM direction

On Fig. S3, we provide a zoom of the SE x +DDMFT and LDA+DMFT spectral functions in the very low-energy region around the Fermi level. Even though at this scale the numerical precision becomes challenging, the momentum-dependent corrections to the flat low-energy band and the Fermi surface induced by the screened exchange terms are clearly visible.

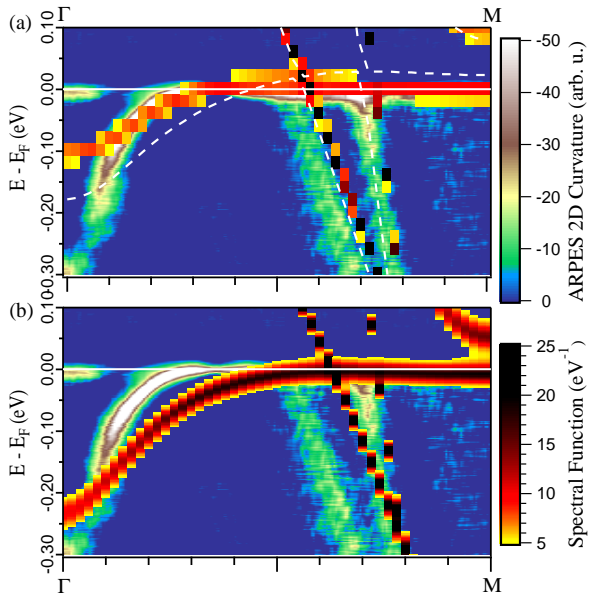


Figure S3: Quasi-particle dispersion near the Fermi surface along the ΓM direction, extracted from the spectral function calculated by (a) SEEx+DDMFT and (b) LDA+DMFT, superimposed on ARPES data as in Fig. 4 of the main text. The QSGW band structure is also given (white dashed lines). The Fermi level is indicated by the solid white line.

C. Co- $d_{x^2-y^2}$ orbital character

As a further support for the interesting physics related to the Co- $d_{x^2-y^2}$ orbital, we display on Figure S4 the orbital-resolved LDA band structure and SEEx+DDMFT spectral function for this orbital character. We can see that indeed the lowest Co- d band is in majority of $d_{x^2-y^2}$ character, as well as the flat band near the Fermi level. This is in contrast to the iron pnictides, in which the Fermi level lies in-between those bonding and non-bonding $d_{x^2-y^2}$ bands, such that there are no $d_{x^2-y^2}$ states at the Fermi surface. On the other hand, the electron pockets near the M point are, similarly to iron pnictides, of d_{xy} and d_{xz+yz} character. As a result, the extension of the electron pockets near M and the contraction of the electron pocket near Γ caused by the non-local screened exchange is at the origin of the reduction of the number of electrons in the $d_{x^2-y^2}$ orbital.

D. Further perspectives

We finally comment on two remaining discrepancies between our theoretical spectral functions and the ARPES spectra of Fig. 4 (main text). At one fourth of the ΓM path, the isolated feature at -0.4 eV is probably due to spin-orbit coupling, as a QSGW calculation with spin-orbit interactions (not shown) lets us foresee. Around the X point (see Fig. 3(b) of the main text),

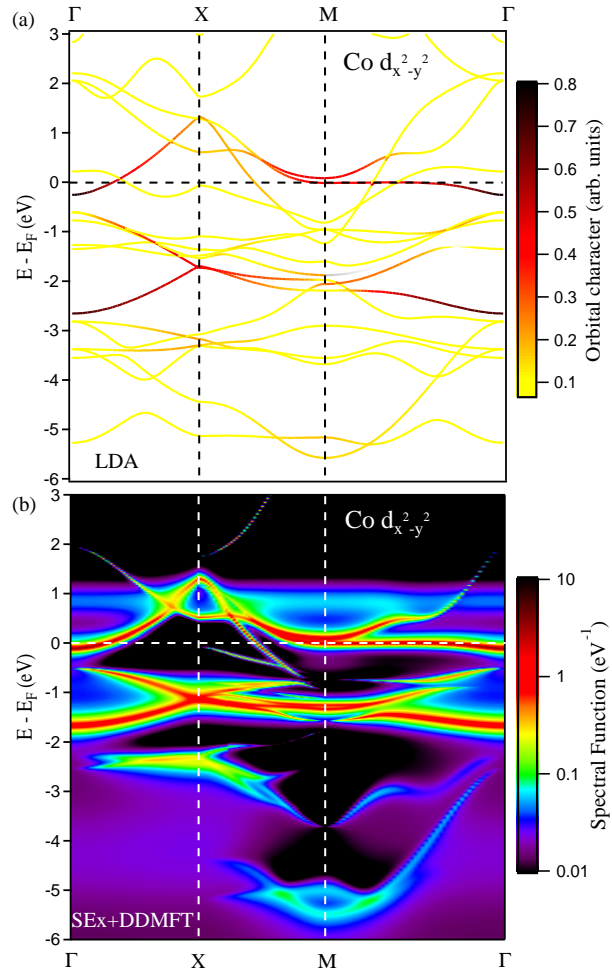


Figure S4: Co- $d_{x^2-y^2}$ orbital character in (a) LDA bands and (b) SEEx+DDMFT spectral function.

our theoretical data does not match the Fermi surface deduced from the ARPES spectrum. However, we note that this point is not a high-symmetry point and it is consequently difficult to identify it with certainty. Moreover, the ARPES cuts correspond to a single photon energy, and in the free electron final state approximation for a given photon and binding energy the sum $k_{\perp}^2 + k_{\parallel}^2$ is constant. This means in our case that for the “ $k_z = 0$ ” cut the k_z at the M point is actually lower by about $0.32\pi/c'$ compared to the Γ point and at the X point it is about $0.16\pi/c'$ lower (where c' is the distance between two CoAs planes). Given the precision of our comparison, we consider that we might be within the error bars. Further combined ARPES and SEEx+DDMFT studies will be needed to assess the respective limitations in precision inherent to theory and experiments.

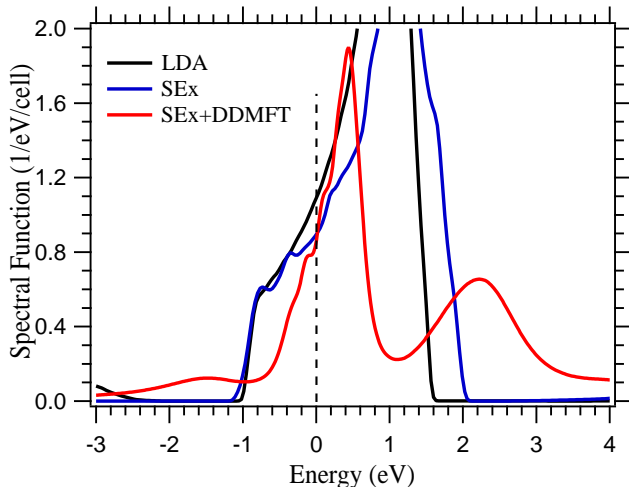


Figure S5: Comparison of the SEEx+DDMFT spectral function of the t_{2g} states of SrVO₃ (red) with the t_{2g} density of states within LDA (black) and SEEx (blue).

III. APPLICATION TO SRVO₃

As support to our new SEEx+DDMFT scheme, we provide in this paragraph a benchmark on a classical transition metal oxide: SrVO₃, a cubic perovskite compound in the correlated metal regime, can be considered as a drosophila system of strongly correlated materials. We use the dynamical interactions as calculated within cRPA (see e.g. [S2]), corresponding to a zero-frequency value of $U(\omega = 0) = 3.5$ eV, and a dynamical tail leading to a bosonic renormalization factor of $Z_B = 0.7$. The screening wavevector is estimated to be $k_{TF} = 1.1 a_0^{-1}$ from the SEEx density of states. For SrVO₃, with three fully degenerate t_{2g} -states, this value corresponds by construction to the self-consistent density of states (differing only slightly from the LDA screening wavevector of $k_{TF} = 1.2 a_0^{-1}$). In Fig. S5, we display the density of states of the t_{2g} orbitals within DFT-LDA and SEEx compared to the spectral function obtained within SEEx+DDMFT. We observe the well-known three-peak structure with a renormalized quasi-particle peak and upper and lower Hubbard bands. However, at variance with LDA+DMFT spectra, the po-

sition of the upper Hubbard band is decreased in energy, locating it at energies slightly larger than 2 eV. This is consistent with the findings in GW +DMFT calculations [S2], which predict an upper Hubbard band at this energy, identifying the pronounced peak at 2.7 eV seen in inverse photoemission spectroscopy [S13] as resulting from $V-e_g$ states. The compensation effect between non-local screened-exchange and the dynamical tail discussed above for BaCo₂As₂ is confirmed also in this case. A more detailed account of these calculations will be published in Ref. [S14].

* Electronic address: vanroeke@cphpt.polytechnique.fr

- [S1] J. M. Tomczak, M. van Schilfgaarde, and G. Kotliar, Phys. Rev. Lett. **109**, 237010 (2012).
[S2] J. M. Tomczak, M. Casula, T. Miyake, and S. Biermann, Phys. Rev. B **90**, 165138 (2014).
[S3] P. Werner and A. J. Millis, Phys. Rev. Lett. **104**, 146401 (2010).
[S4] M. Casula, P. Werner, L. Vaugier, F. Aryasetiawan, T. Miyake, A. J. Millis, and S. Biermann, Phys. Rev. Lett. **109**, 126408 (2012).
[S5] P. Blaha, K. Schwarz, G. Madsen, D. Kvasnicka, and J. Luitz, *Wien2k, An Augmented Plane Wave+Local Orbitals Program for Calculating Crystal Properties* (Tech. Universität Wien, Austria, 2001).
[S6] F. O. Tran and P. Blaha, Phys. Rev. B **83**, 235118 (2011).
[S7] L. Vaugier, H. Jiang, and S. Biermann, Phys. Rev. B **86**, 165105 (2012).
[S8] L. Vaugier, Ph.D. thesis, Ecole Polytechnique, France (2011).
[S9] P. Werner, M. Casula, T. Miyake, F. Aryasetiawan, A. J. Millis, and S. Biermann, Nature Physics **8**, 331 (2012).
[S10] V. I. Anisimov, J. Zaanen, and O. K. Andersen, Phys. Rev. B **44**, 943 (1991).
[S11] S. Biermann, F. Aryasetiawan, and A. Georges, Phys. Rev. Lett. **90**, 086402 (2003).
[S12] L. Hedin, J. Phys. Condens. Matter **11**, R489 (1999).
[S13] K. Morikawa, T. Mizokawa, K. Kobayashi, A. Fujimori, H. Eisaki, S. Uchida, F. Iga, and Y. Nishihara, Phys. Rev. B **52**, 13711 (1995).
[S14] A. van Roekeghem and S. Biermann, EPL **108**, 57003 (2014).